



UNIVERSITY OF LEEDS

This is a repository copy of *Novel double-layer DC/AC railway traction power supply system with renewable integration*.

White Rose Research Online URL for this paper:  
<http://eprints.whiterose.ac.uk/167820/>

Version: Accepted Version

---

**Article:**

Li, Y, Li, K [orcid.org/0000-0001-6657-0522](https://orcid.org/0000-0001-6657-0522), Zhang, L et al. (1 more author) (2020) Novel double-layer DC/AC railway traction power supply system with renewable integration. *IET Renewable Power Generation*, 14 (18). pp. 3616-3627. ISSN 1752-1416

<https://doi.org/10.1049/iet-rpg.2020.0131>

---

© The Institution of Engineering and Technology 2020. This is an author produced version of an article accepted for publication in *IET Renewable Power Generation*. Uploaded in accordance with the publisher's self-archiving policy.

**Reuse**

Items deposited in White Rose Research Online are protected by copyright, with all rights reserved unless indicated otherwise. They may be downloaded and/or printed for private study, or other acts as permitted by national copyright laws. The publisher or other rights holders may allow further reproduction and re-use of the full text version. This is indicated by the licence information on the White Rose Research Online record for the item.

**Takedown**

If you consider content in White Rose Research Online to be in breach of UK law, please notify us by emailing [eprints@whiterose.ac.uk](mailto:eprints@whiterose.ac.uk) including the URL of the record and the reason for the withdrawal request.



[eprints@whiterose.ac.uk](mailto:eprints@whiterose.ac.uk)  
<https://eprints.whiterose.ac.uk/>

---

# A Novel Double-layer DC/AC Railway Traction Power Supply System with Renewable Integration

Yongfei LI<sup>1</sup>, Kang LI<sup>2</sup>, Li ZHANG<sup>2</sup>, Yong LI<sup>1\*</sup>

<sup>1</sup> School of Electrical Engineering and Automation, Harbin Institute of Technology, Harbin, China

<sup>2</sup> School of Electronic and Electrical Engineering, University of Leeds, Leeds, United Kingdom

\* E-mail: liyong611@hit.edu.cn

**Abstract:** Back-to-back converter based railway traction power supply system (TPSS) can eliminate neutral sections in the traction side and improve power quality in the grid side, but it still has some drawbacks such as low reliability, difficulty in accepting large-capacity renewable energy, and power mismatches. In this paper, a double-layer DC/AC TPSS with renewable integration is proposed to address these challenges and to improve system performance. The proposed topology breaks the limit of back-to-back structure and enables more flexible free energy flow. A top-down system design method is proposed in this paper. Firstly, the characteristics of the proposed TPSS for integration with renewable power are described and compared with the traditional back-to-back topology. Secondly, a DC droop controller and a AC droop controller are designed for DC layer grid and AC layer grid respectively to control the power flow in each layer. The traditional AC droop control is based on the inductive transmission impedance, but the resistance of traction transmission line cannot be ignored. Thus a modified droop control strategy with the consideration of line resistance is also proposed in this paper. Subsequently, the voltage control strategy for the single MMC converter is designed to track the reference signal from the upper droop controller. Finally, a general double-layer DC/AC TPSS is designed from bottom to top, and the simulation results confirm that the proposed TPSS with renewable integration is capable of delivering desirable performance.

---

## 1 Introduction

Compared with traditional diesel locomotives, modern electric locomotives have the advantages of low noise, low environmental pollution, and high efficiency [1]. The traction power supply system (TPSS) provides energy for the operation of electrified railway, and the power quality of TPSS is directly related to the safety, reliability and economy of the whole railway system [1, 2]. The electrified railway adopts the single-phase AC power supply system. The traction substation obtains the electric energy from the three-phase public grid, and through the transformer, the three-phase voltage is transformed into two separate single-phase AC voltages to feed the traction networks [3]. In the traditional TPSS, there are two main drawbacks: i) neutral sections in the traction side. The current TPSS adopts a sectionalized power supply mode. Different sections are supplied by different phases of the power grid, resulting in inconsistent voltage phase between adjacent sections. Therefore, neutral sections are essential, yet the electrical dead zone in neutral sections will inevitably bring speed loss, electric shock and other adverse effects [4]. ii) power quality in the grid side. Since the TPSS is directly connected to the public power grid, the varying traction loads will introduce power quality issues such as the negative-sequence current, reactive power and harmonics, which seriously affect the power quality of the public grid and limits the further development of traction capacity [1].

With the development of modern power electronics technology, it is possible to use advanced power electronics to solve the issues in the existing TPSS [5]. In the literature, a number of researches have been conducted to utilize the power electronics technology to improve the performance of TPSS. In [3], the negative sequence current in transformer based TPSS is analyzed, and a railway power conditioner (RPC) is proposed to suppress the unbalanced current. A single-phase back-to-back active power compensator (APC) is proposed in [6]. In this topology, the two outputs of the transformer are connected by APC for active power balance, reactive power compensation, and harmonics suppression. Two parallel APCs have been successfully applied in an actual 10 MVA/27.5 kV co-phase system in Meishan substation, Chengdu, China [7]. Since the APC

based co-phase system has the ability of active power balance and reactive power compensation, the conventional transformer based dual-branch power supply topology can be replaced by one-branch scheme, and the neutral section at the substation can be eliminated. In order to reduce the operating voltage, a hybrid power quality conditioner (HPQC) with a LC branch is proposed in [8]. Compared to the APC scheme, its DC voltage is reduced by around 20%. In [9], optimal parameter design of HPQC is presented, and the detailed mathematical derivation is also presented.

The utilization of power electronics in TPSS improves the performance of the traditional TPSS to some extent, but it cannot completely solve the existing problems. Since the supply voltage comes from the transformer and cannot be controlled, the neutral section between substations is still required. Therefore, full power electronics based power supply systems have been proposed. In [2], an advanced co-phase TPSS is proposed in which three-phase to single-phase back-to-back converters are used. Different from transformer based TPSS, back-to-back converters based TPSS can control the phase angle of the output voltage, so that multiple split power supply sections can be connected together, and neutral sections can be eliminated. In [10], a novel back-to-back topology based on multiple converters is proposed and applied in TPSS, it can meet the high power demand of the traction system. A novel TPSS based on modular multilevel converters (MMC) is proposed in [4], both the mathematical model and control strategy of the MMC converter are presented. The above researches mainly focus on the modelling and control of a single power electronic converter. There is a lack of system-level operation study on the full power electronics based TPSS. In [4], the conventional AC droop control scheme is directly applied to single-phase inverters without the consideration of transmission line impedance. A modified droop control strategy is proposed for railway auxiliary power supply system in [11], but the topology of auxiliary system is different from the full power electronics based TPSS.

While more power electronics are used in the railway systems, the worldwide energy system is also experiencing substantial landscape change due to significant penetration of renewable generations [12–14]. The forecasting and control of renewable generation have

made significant progress in recent years [15, 16]. The new developments in both renewable energies and electrified railways have brought new opportunities and challenges. Different configurations to integrate renewable energies into TPSS are compared in terms of control performance and economic benefits in [17]. In [18], a single-phase back-to-back PV generation system and associated control scheme are proposed. In this topology, the back-to-back converter can transfer PV energy to the traction network and dynamically adjust its output current according to the real-time traction loads, so as to achieve active power balance and reactive power compensation.

The power electronic converter controls the energy conversion in TPSS. Compared with the traditional two-level or three-level voltage source converter (VSC), the modular multilevel converter (MMC) has the characteristics of multilevel voltage output, flexible voltage level control, low harmonic content, and low switching loss [19]. MMC has been widely studied and applied in the field of HVDC transmission and the conversion of high-voltage energy [20], and shows a promising prospect in the future TPSS [21]. A railway traction power conditioner (RPC) based on MMC is proposed to reduce three-phase unbalance for the high-speed railway system [22]. Similarly, a multilevel railway power conditioner (RPC) is proposed in [23], and a sliding mode current controller is also designed. In recent years, many MMC based RPCs have been proposed for power balancing. In Ref. [24], RPCs with different topologies are compared for an optimal selection. In addition to the back-to-back converter, a direct single-phase AC/AC modular multilevel converter, in which full bridge submodule is used, is also developed to solve the issues caused by unbalanced traction loads [25]. For the 16.7Hz railway system in Germany, a direct three-phase to single-phase AC/AC MMC scheme is proposed [26].

In this paper, a double-layer DC/AC TPSS is proposed to allow better integration of renewable power, and the control scheme of system operation is designed to improve the system performance. The remainder of this paper is organized as follows. The topology and renewable integration of the proposed system are presented and compared with the back-to-back scheme in Section II. A DC droop controller and a modified AC droop controller are designed for the DC layer and AC layer respectively in Section III. The mathematical model and control scheme of the MMC rectifier and inverter are derived in Section IV. A general double-layer DC/AC TPSS is established in Section V, and the system control strategy is verified by simulation results. Finally, Section VI concludes the paper.

## 2 Double-layer DC/AC TPSS with Renewable Integration

The purpose of this paper is to build and operate a full converter based TPSS, including system topology analysis, renewable integration, system control and converter control. With the emergence of high-power converters and the development of modern control technology, the concept of full power electronics based TPSS has been proposed in recent years [2, 4, 10]. Fig. 1(a) shows a typical back-to-back converter based TPSS topology proposed in [2, 10]. In this topology, each back-to-back converter acts as a separate unit, and all back-to-back units are connected in parallel between the public grid and traction network. Compared with the traditional transformer based TPSS, this is a more ideal traction power supply system, and the main advantages of back-to-back topology can be summarized as follows:

- Eliminate neutral sections and share energy on the traction side. Since both the amplitude and phase angle of the inverter output voltage can be fully controlled, all neutral sections can be removed. The traction load is powered by multiple parallel back-to-back units, leading to energy sharing and capacity reduction.
- Reduce power pollution and improve power quality on the grid side. Due to the decoupling effect of DC bus, only the active power will be transferred to the MMC rectifiers, so the injected currents can be balanced, reducing the negative consequences of reactive power, negative-sequence current and harmonics. On the other hand, an extra current can be generated to eliminate the original harmonics in the public grid, thus improving power quality.

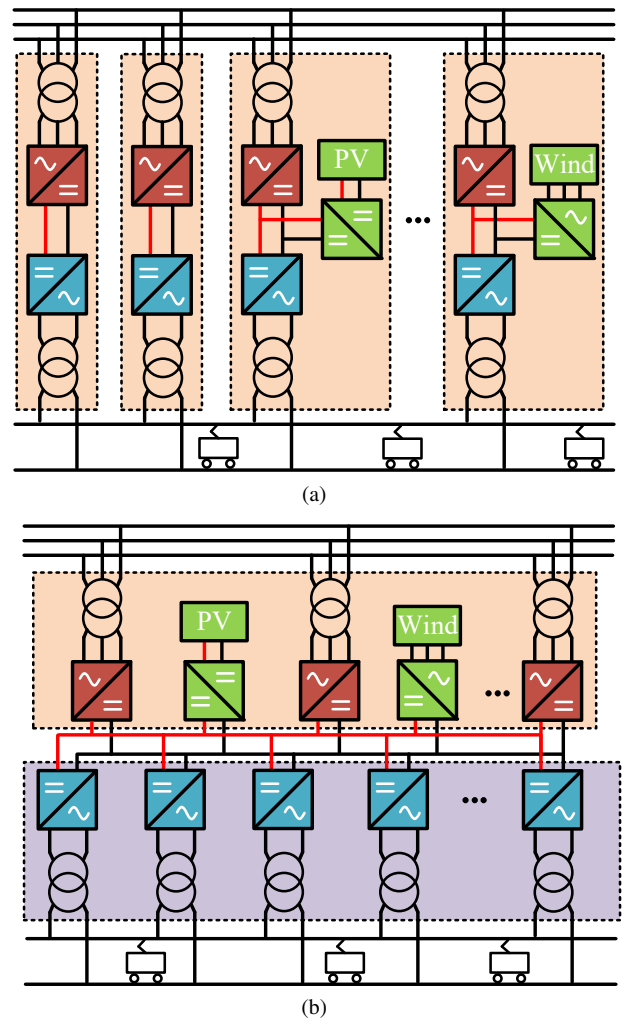


**Fig. 1:** Full power electronics based TPSS with renewable integration. (a) Back-to-back topology. (b) Double-layer DC/AC topology.

- Integrate renewable energy. The existence of DC bus in back-to-back converter enables renewable integration. Fig. 1(a) shows the integration of photovoltaic and wind energy. The back-to-back converter works as the grid-connected circuit of renewable generation, so that the cost of renewable generation is reduced.

As elaborated earlier, the concept of back-to-back converter based TPSS can effectively solve the existing problems in the traditional transformer based TPSS. However, it also has its own disadvantages:

- Low reliability. Due to the physical constraint of back-to-back structure, each rectifier works with an inverter as a back-to-back unit. When either the rectifier or the inverter fails, the other in this unit will also fail.
- Limits on accepting large scale renewable power. The allowable capacity of renewable generation depends on the maximum power of the back-to-back unit, which limits the integration of large-capacity renewable energy in traction system.
- Power mismatches. In power electronic based TPSS, the grid-connected rectifier is a three-phase converter, while the traction-connected inverter is a single-phase converter. Therefore, if these converters adopt the same IGBT submodules, the rated rectifier power would be around 1.5 times of the rated inverter power. Besides, the introduction of renewable energy will further aggravate power mismatches, resulting in the waste of converter capacity, thus increasing the investment costs.

In [4], a power supply structure with a DC bus is briefly introduced, which consists of a rectifier and several inverters in the common bus. However, it primarily focuses on the development of control strategy for a single converter, the whole system operation performance is not considered, and the issues in back-to-back topology is not analyzed systematically. In order to overcome the drawbacks of back-to-back topology, a double-layer DC/AC TPSS topology with renewable integration is proposed in this paper, as shown in Fig. 1(b). This topology is composed of both a DC layer and a AC layer. The number and location of the converters in each layer is flexible, and free from the limits of back-to-back structure. Compared with back-to-back topology, it has the following distinctive features:

- The benefits of back-to-back topology are retained. Both on the traction side and grid side, converters are still the interface for energy conversion. Therefore, the advantages brought by power electronics, such as neutral section elimination and power quality improvement, are preserved.
- Substation fault ride through ability is enhanced. All converters are connected to the DC-layer network, and the energy can flow freely in the DC network. Different converters can share energy and support each other, so even if a converter fails, the others can still work without being affected.
- Large-capacity renewable energy can be effectively integrated. The energy in the DC grid can be shared by multiple converters. So the capacity required for renewable integration can be easily shared by all converters in this DC network.
- Power distribution can be optimized. The configuration of double-layer TPSS is very flexible without the spatial limit of back-to-back structure. The number and location of the rectifiers can be re-designed by optimization methods based on the actual situations. In addition, the characteristics of renewable generations can also be considered in the optimization process to mitigate potential negative effects.

The proposed structure has many merits but also brings forward some challenges, including:

- Economically, the newly introduced DC layer grid will inevitably increase the construction cost, thus the economic optimization needs to be considered in the early planning stage.
- Technically, the DC-layer grid not only provides more channels for power flow, but also leads to harmonic interference. Besides, DC protection, especially for short circuit faults in large-scale networks, should also be considered in the future works.

The main purpose of this paper is to present a new double-layer traction power supply topology and its overall control scheme, from single MMC control to parallel power sharing control, and to verify the feasibility, especially for renewable integration and substation fault ride through.

### 3 Droop Control

Compared with the sectionalized power supply mode in conventional transformer based TPSS, the proposed double-layer TPSS adopts interconnected power supply mode. All MMC rectifiers are connected in parallel to form the DC-layer grid, and MMC inverters are also connected in parallel to power traction loads. Energy flow control in DC-layer and AC-layer grid is the foundation of system operation. Droop control can achieve the purpose of power distribution even without communication, and the power supply system based on droop control shows high reliability [27]. Therefore, droop control is adopted to realize the primary control of energy flow in both DC-layer and AC-layer grid.

#### 3.1 DC Droop Control

In the DC-layer grid, the bus voltage is the result of parallel rectifier operation. The energy flow for each rectifier can be controlled by adjusting its output voltage. A typical schematic diagram of power

transmission is shown in Fig. 2, where  $U_{DCi}$  is the output voltage of  $i$ -th AC-DC converter,  $R_i$  is the line resistance from the converter to the load,  $P_i$  is the transmitted power, and  $V_{DC0}$  is the load voltage as a reference voltage. The relationship between these variables can be easily obtained as

$$P_i = U_{DCi} \frac{U_{DCi} - V_{DC0}}{R_i}. \quad (1)$$

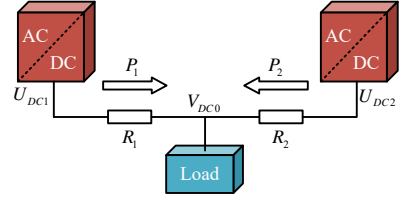


Fig. 2: Schematic diagram of power transmission in DC-layer grid

The only controllable variable that can be used to change the power is the output voltage. The relationship between voltage variation and power variation can be derived as

$$\Delta P = \Delta U \left. \frac{dP}{dU} \right|_{U_{DC0}} = \Delta u \frac{V_{DC0} (2U_{DC0} - V_{DC0})}{R}, \quad (2)$$

where  $\Delta u = \Delta U / V_{DC0}$ ,  $U_{DC0}$  is the output voltage at the current moment. Considering that power changes are mainly caused by voltage changes and ignoring the slight difference between converter output voltage and load voltage, the above equation can be simplified to

$$\Delta P \approx \frac{V_{DC0}^2}{R} \Delta u. \quad (3)$$

It can be seen that power increment is proportional to voltage increment. In order to achieve a rational energy flow, the reference voltage of a parallel converter can be obtained by (4). The relationship between the reference voltage and the feedback power is shown in Fig. 3. When the output power of a converter keeps increasing, its output voltage will be adjusted downward which would slow down power growth rate and stabilize it within the rated power range.

$$u^* - u_0 = - \frac{u_{\max} - u_{\min}}{P_{\max} - P_{\min}} (P - P_0) \quad (4)$$

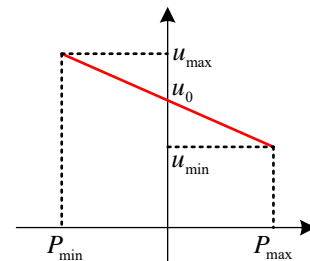


Fig. 3: DC droop curve

The internal control of a AC-DC converter consists of voltage and current loop control. So the general realization of droop control in the DC-layer grid is: droop control is introduced as an external controller to provide a reference DC voltage, and then the reference signal will be tracked by the double closed-loop controller. The specific control block diagram is shown in Fig. 4.

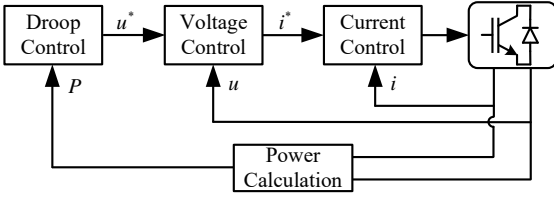


Fig. 4: Block diagram of overall DC droop control

### 3.2 Conventional AC Droop Control

Conventional AC droop control realizes the parallel operation of distributed generations by emulating droop characteristics of a synchronous generator. The realization of AC droop control is similar to DC droop control. The difference is that both the voltage amplitude and phase need to be controlled. The traditional droop control for a converter is give by

$$f - f_0 = -\frac{f_{\max} - f_{\min}}{P_{\max} - P_{\min}} (P - P_0) = -k_p (P - P_0), \quad (5a)$$

$$u - u_0 = -\frac{u_{\max} - u_{\min}}{Q_{\max} - Q_{\min}} (Q - Q_0) = -k_q (Q - Q_0), \quad (5b)$$

where  $f_0$  and  $u_0$  are the rated frequency and voltage,  $P_0$  and  $Q_0$  are the rated active and reactive power,  $P_{\min}$ ,  $Q_{\min}$  and  $P_{\max}$ ,  $Q_{\max}$  are lower and upper limits of active and reactive power, and  $f_{\min}$  and  $f_{\max}$  are the minimum and maximum allowable frequency. According to equation (5), the block diagram of conventional AC droop control is shown in Fig. 5.

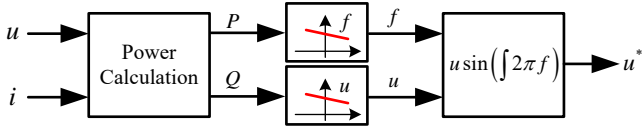


Fig. 5: Conventional AC droop control scheme

The traditional droop control is derived when the line inductive reactance is much greater than the line resistance. This assumption of a mainly inductive line impedance is suitable for high-voltage transmission applications [28]. However, for the medium-voltage traction power supply systems, the ratio of resistance to reactance, in different situations and under different load current conditions, ranges from 0.39 to 1.42 [29–31], meaning that line resistance cannot be ignored. Thus a modified droop control scheme with the consideration of line resistance is required for parallel operation in traction power supply systems.

### 3.3 Modified AC Droop Control for TPSS

In AC traction system, the line resistance can not be neglected, so the single input single output (SISO) relationship of  $P$ - $f$  and  $Q$ - $u$  is no longer valid. Different variables are coupled with each other, forming a multiple input multiple output (MIMO) control system. In AC TPSS, the equivalent power transmission diagram is shown in Fig. 6, where  $V_{AC0}$  is the load voltage as a reference value,  $U_{ACi} \angle \delta_i$  is the output voltage of  $i$ -th converter,  $R_i + jX_i$  is the line impedance and can be written as  $Z_i \angle \theta_i$ . The transmitted active and reactive power can be obtained as:

$$P = \frac{U}{R^2 + X^2} (UR - V_0 R \cos \delta + V_0 X \sin \delta), \quad (6a)$$

$$Q = \frac{U}{R^2 + X^2} (UX - V_0 R \sin \delta - V_0 X \cos \delta). \quad (6b)$$

It can be seen that active and reactive power are related to both the voltage amplitude and phase angle. So the power increment can be

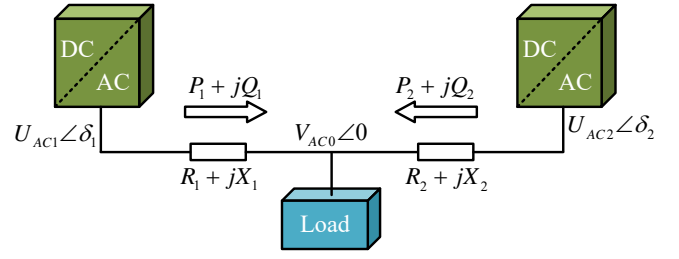


Fig. 6: Schematic diagram of power transmission in AC-layer grid

derived by the increment of amplitude and phase angle, as shown in (7a) and (7b), where  $U_0 \angle \delta_0$  is the output voltage at current moment.

$$\Delta P = \Delta U \left. \frac{\partial P}{\partial U} \right|_{U_0, \delta_0} + \Delta \delta \left. \frac{\partial P}{\partial \delta} \right|_{U_0, \delta_0} \quad (7a)$$

$$\Delta Q = \Delta U \left. \frac{\partial Q}{\partial U} \right|_{U_0, \delta_0} + \Delta \delta \left. \frac{\partial Q}{\partial \delta} \right|_{U_0, \delta_0} \quad (7b)$$

From the above equations, the expression of active and reactive power variation can be derived,

$$\begin{aligned} \Delta P = \Delta u \frac{V_0}{R^2 + X^2} (2U_0 R - V_0 R \cos \delta_0 + V_0 X \sin \delta_0) \\ + \Delta \delta \frac{U_0}{R^2 + X^2} (V_0 R \sin \delta_0 + V_0 X \cos \delta_0), \end{aligned} \quad (8a)$$

$$\begin{aligned} \Delta Q = \Delta u \frac{V_0}{R^2 + X^2} (2U_0 X - V_0 R \sin \delta_0 - V_0 X \cos \delta_0) \\ + \Delta \delta \frac{U_0}{R^2 + X^2} (-V_0 R \cos \delta_0 + V_0 X \sin \delta_0). \end{aligned} \quad (8b)$$

where  $\Delta u = \Delta U / V_0$ . It is worth noting that, since both the resistance and inductance are approximately proportional to the length of transmission line, the impedance angle  $\theta$  can be considered to remain constant during the train movement. Ignore the slight difference between  $U_0 \angle \delta_0$  and  $V_0 \angle 0$ , (8) can be simplified as

$$\Delta P = \frac{V_0^2}{\sqrt{R^2 + X^2}} (\Delta u \cos \theta + \Delta \delta \sin \theta), \quad (9a)$$

$$\Delta Q = \frac{V_0^2}{\sqrt{R^2 + X^2}} (\Delta u \sin \theta - \Delta \delta \cos \theta). \quad (9b)$$

It is evident that both the voltage amplitude and phase angle have effects on active power and reactive power, and the line impedance angle represents the weight coefficient. This is to say, the coupling between the output voltage and power is related by the impedance angle. The coupling relationships between power variation and voltage variation when  $\theta = \frac{\pi}{2}$  and  $\theta = \frac{\pi}{4}$  are compared in Fig. 7. The SISO relationship when  $\theta \approx \frac{\pi}{2}$  is illustrated in Fig. 7(a) and Fig. 7(b). However, in AC TPSS, the line resistance can not be ignored, so the coupling effect should be considered. According to (9), a modified droop control scheme with the consideration of impedance phase angle is proposed as

$$(u - u_0) \cos \theta + (f - f_0) \sin \theta = -k_p (P - P_0), \quad (10a)$$

$$(u - u_0) \sin \theta - (f - f_0) \cos \theta = -k_q (Q - Q_0). \quad (10b)$$

For the convenience of implementation, the above equation is transformed, and the reference voltage can be calculated by (11).

$$f - f_0 = -k_p \sin \theta (P - P_0) + k_q \cos \theta (Q - Q_0) \quad (11a)$$

$$u - u_0 = -k_p \cos \theta (P - P_0) - k_q \sin \theta (Q - Q_0) \quad (11b)$$

The impedance phase angle represents the weight of active power and reactive power. When  $\theta = \frac{\pi}{2}$ , equation (11) can be simplified to the conventional droop control.

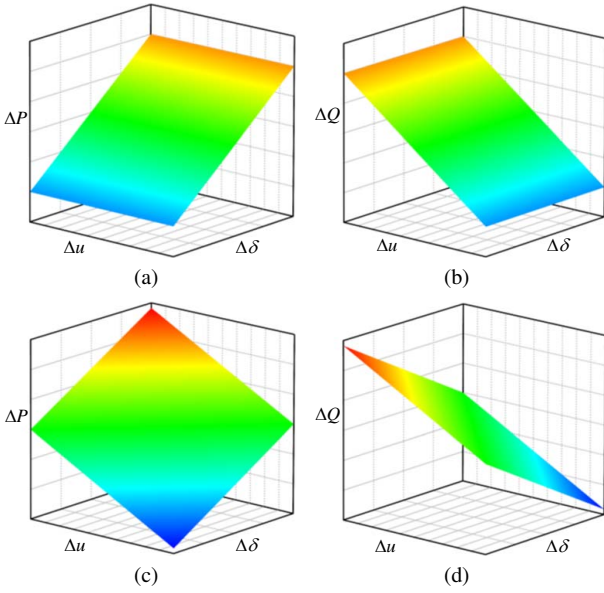


**Fig. 7:** The coupling relationship between power variation and voltage variation with different line impedance angles. (a) Active power when  $\theta = \frac{\pi}{2}$ . (b) Reactive power when  $\theta = \frac{\pi}{2}$ . (c) Active power when  $\theta = \frac{\pi}{4}$ . (d) Reactive power when  $\theta = \frac{\pi}{4}$ .

## 4 MMC Control

The control of an individual MMC needs to consider a number of aspects, such as output voltage and current tracking performance [32], internal circulating current suppression [33], capacitor voltage fluctuations [34], admittance modelling [35], and short-circuit current protection [36], etc. Since this paper aims to develop the proposed TPSS to address renewable integration and substation fault ride through, therefore the MMC output voltage control and internal circulating current control are the main focus in this paper. Note that, if it comes to the protection system design and quantitative stability analysis, then the circuit current [36, 37] and admittance modelling [35, 38] of MMC should also be considered.

### 4.1 MMC Rectifier Control

Fig. 8 shows the topology of three-phase MMC rectifier, which is composed of six bridge arms. Each arm consists of several submodules (SM), an arm inductor  $L_0$  and an equivalent resistor  $R_0$ , and the overall arm impedance is denoted as  $Z_0$ . Similarly, the grid-connected impedance is denoted as  $Z_g$ , which consists of  $L_g$  and  $R_g$ .

The output voltage of each submodule is zero or capacitor voltage  $u_c$ , so the available voltage for each arm is  $0-Nu_c$ . The KVL equations for the positive arm and negative arm of each phase are derived as follows:

$$u_{gj} + Z_g i_{gj} + u_{pj} + Z_0 i_{pj} = 0.5u_{dc}, \quad (12a)$$

$$u_{gj} + Z_g i_{gj} - u_{nj} - Z_0 i_{nj} = -0.5u_{dc}, \quad (12b)$$

where  $Z_g = R_g + sL_g$  ( $s$  is the differential operator);  $Z_0 = R_0 + sL_0$ ,  $u_{dc}$  is the DC output voltage;  $u_{gj}$  is the grid voltage of phase  $j$  ( $j = a, b, c$ );  $u_{pj}$ ,  $u_{nj}$  are the output voltage of positive arm and the negative arm of phase  $j$  ( $j = a, b, c$ );  $i_{pj}$ ,  $i_{nj}$  are the arm currents; their positive direction is defined as shown in Fig. 8.

According to KCL,  $i_{gj} = i_{pj} - i_{nj}$  ( $j = a, b, c$ ), so equation (12) can be rewritten as:

$$(R + sL) i_{gj} = u_{difj} - u_{gj}, \quad (13a)$$

$$(R_0 + sL_0) i_{cirj} = 0.5u_{dc} - u_{comj}. \quad (13b)$$

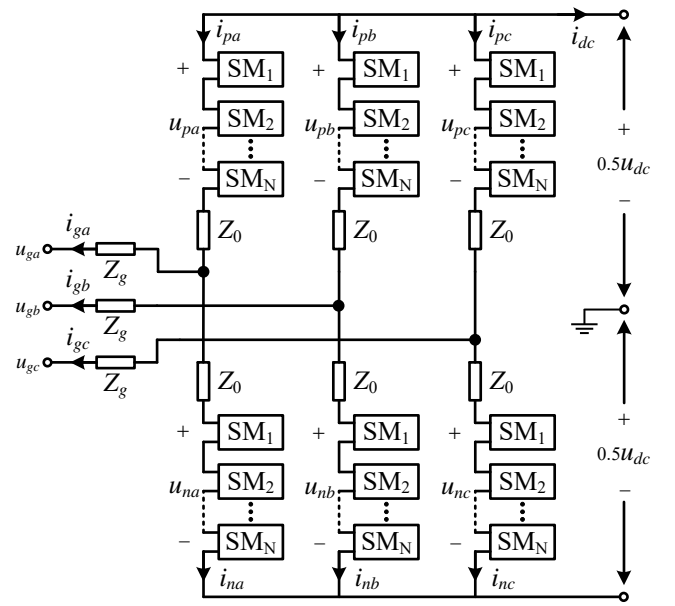


**Fig. 8:** MMC rectifier topology

where  $L = L_g + 0.5L_0$ ,  $R = R_g + 0.5R_0$ ,  $u_{comj}$  and  $u_{difj}$  are the common and differential voltage respectively, defined as:

$$\begin{cases} u_{comj} = 0.5(u_{nj} + u_{pj}) \\ u_{difj} = 0.5(u_{nj} - u_{pj}) \end{cases} \quad (14)$$

According to (13a), the dynamic equation of the grid current in  $abc$ -coordinate system can be written as:

$$\begin{cases} (R + sL) i_{ga} = u_{difa} - u_{ga} \\ (R + sL) i_{gb} = u_{difb} - u_{gb} \\ (R + sL) i_{gc} = u_{difc} - u_{gc} \end{cases} \quad (15)$$

It can be seen that the phase current of power grid can be controlled by the differential voltage of MMC, transform it into  $dq$ -coordinate system,

$$\begin{cases} (R + sL) i_{gd} = \omega L i_{gq} + u_{difd} - u_{gd} \\ (R + sL) i_{gq} = -\omega L i_{gd} + u_{difq} - u_{gq} \end{cases} \quad (16)$$

Through Park transformation, the three-phase sinusoidal signal is converted into a dc signal under two orthogonal phases. And the reference value of  $dq$ -axis differential voltage can be calculated by (17), and the overall control diagram of the grid current is shown in Fig. 9.

$$\begin{cases} u_{difd}^* = \left( k_{p1} + \frac{k_{i1}}{s} \right) (i_{gd}^* - i_{gd}) - \omega L i_{gq} + u_{gd} \\ u_{difq}^* = \left( k_{p1} + \frac{k_{i1}}{s} \right) (i_{gq}^* - i_{gq}) + \omega L i_{gd} + u_{gq} \end{cases} \quad (17)$$

where  $i_{gd}^*$  and  $i_{gq}^*$  are the  $d$ -axis and  $q$ -axis reference current respectively.

The active power exchange between the MMC rectifier and the outside will change the overall capacitor energy. Since the capacitor energy of MMC rectifier is directly related to the DC output voltage, the DC voltage control is realized by active power control. According to the positive direction defined in Fig 8, the instantaneous power absorbed by a MMC rectifier can be calculated by

$$p_{in} = -1.5u_{gd}i_{gd} + u_{dc} \sum i_{cirj} \quad (18)$$

where  $i_{cirj}$  is the circulating current of phase  $j$  ( $j = a, b, c$ ), defined as  $i_{cirj} = 0.5(i_{pj} + i_{nj})$ , and the coefficient 1.5 indicates the power difference caused by amplitude based Park transformation.

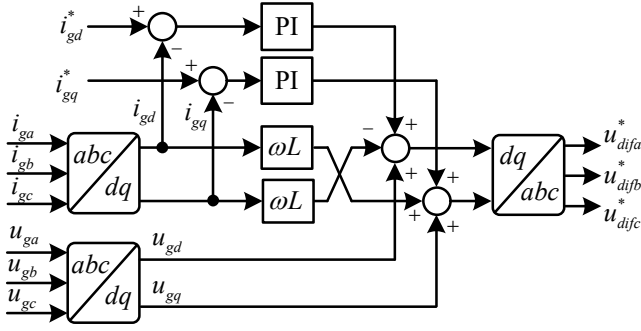


Fig. 9: Control diagram of grid current

Therefore, the DC voltage can be controlled by changing the reference value of the  $d$ -axis current, and the DC load power can be introduced as feed-forward compensation to improve transient response performance. A PI controller is used to eliminate steady state error, so the reference value of  $d$ -axis current can be obtained as

$$i_{gd}^* = - \left( k_{p2} + \frac{k_{i2}}{s} \right) (u_{dc}^* - u_{dc}) + \frac{2}{3} \frac{u_{dc}}{u_{gd}} \sum i_{cirj} \quad (19)$$

where  $u_{dc}^*$  is the reference DC voltage from DC droop controller. The control diagram of DC voltage is shown in Fig. 10.

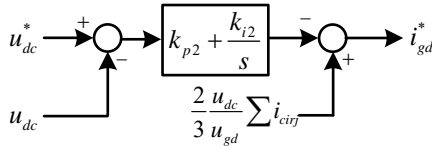


Fig. 10: Control diagram of DC voltage

As shown in Fig. 10,  $i_{gd}^*$  can be obtained by DC voltage control. Since  $i_{gq}$  is related to the reactive power of MMC rectifier,  $i_{gq}^*$  is generally set to zero. However, since the reactive power will not change the overall capacitor energy, the MMC converter can also be used as a static synchronous compensator (STATCOM) to further improve the performance of the public grid. For this case,  $i_{gq}^*$  can be obtained as the output of rectifier power control,

$$i_{gq}^* = \frac{2}{3} \frac{Q_g^*}{u_{gd}} + \left( k_{p3} + \frac{k_{i3}}{s} \right) (Q_g^* - Q_g), \quad (20)$$

where  $Q_g^*$  is the reactive power reference from the grid dispatching center. The control diagram of reactive power control is shown in Fig. 11.

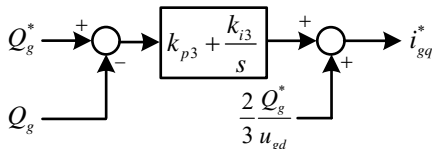


Fig. 11: Control diagram of reactive power

So far, the external dynamics of the MMC rectifier have been controlled. Its output voltage can track the reference signal from droop controller to achieve appropriate energy flow in the DC layer. In order to further improve the performance of the MMC rectifier, its internal dynamics also need to be controlled. Due to the fluctuation of capacitor voltage, a double-frequency circulating current will occur in the three-phase MMC converter, which will not only

increase the loss of MMC converter but also reduce its reliability [39]. According to (13b), the dynamic equation of the circulating current in three phases can be obtained as

$$\begin{cases} (R_0 + sL_0) i_{cira} = 0.5u_{dc} - u_{coma} \\ (R_0 + sL_0) i_{cirb} = 0.5u_{dc} - u_{comb} \\ (R_0 + sL_0) i_{circ} = 0.5u_{dc} - u_{comc} \end{cases} \quad (21)$$

According to (21), the circulating current is related to the common voltage. In the actual operation, it is expected that the three phases can share the energy flow evenly. So the reference values for each circulating current are equal,  $i_{cira}^* = i_{cirb}^* = i_{circ}^* = \frac{1}{3} (i_{cira} + i_{cirb} + i_{circ})$ . It is worth noting that the undesired double frequency component in the three-phase circulating current is symmetric in negative sequence [40]. So in the summation, the double frequency components cancel out each other, and only the desired DC component is retained in the reference signal. In order to eliminate both DC steady-state error and AC steady-state error, a proportional-integral-resonant (PIR) controller is used in this paper, and the reference common voltage for each phase can be calculated by

$$u_{comj}^* = 0.5u_{dc} - \left( k_{p3} + \frac{k_{i3}}{s} + \frac{k_{r3}s}{s^2 + 4\omega_0^2} \right) (i_{cirj}^* - i_{cirj}) \quad (22)$$

where  $j = a, b, c$ ,  $\omega_0$  is the fundamental angular velocity,  $\omega_0 = 100\pi$  rad/s. The control diagram of circulating current is shown in Fig. 12.

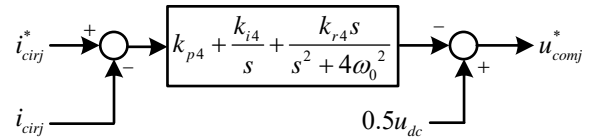


Fig. 12: Control diagram of circulating current in MMC rectifier

The reference differential voltage and common voltage for each phase are generated by the external voltage control and the internal circulating current control respectively. From (14), the reference output voltage of the positive and negative arms can be easily obtained as

$$\begin{cases} u_{pj}^* = u_{comj}^* - u_{difj}^* \\ u_{nj}^* = u_{comj}^* + u_{difj}^* \end{cases} \quad (23)$$

Based on the above analysis, the overall control diagram of the three-phase MMC rectifier is shown in Fig. 13. The outermost  $u_{dc}^*$  and  $Q_g^*$  are from the upper droop controller and the grid dispatching center respectively. While the innermost arm voltages,  $u_{pj}^*$  and  $u_{nj}^*$ , will be modulated into switching signals.

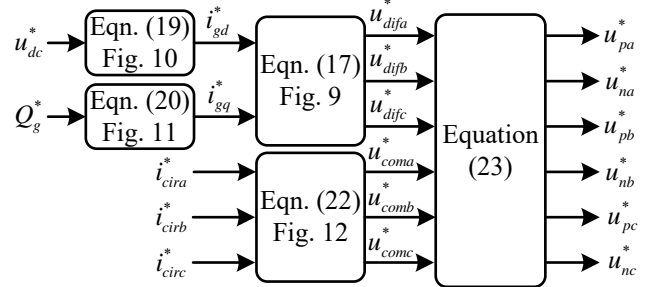


Fig. 13: Overall control diagram of the MMC rectifier

#### 4.2 MMC Inverter Control

Fig. 14 shows the configuration of the single-phase MMC inverter, which is composed of four bridge arms. The configuration and parameters for each arm are exactly the same as those in the MMC rectifier.  $Z_s$  is the equivalent single-phase impedance between the inverter and catenary network.

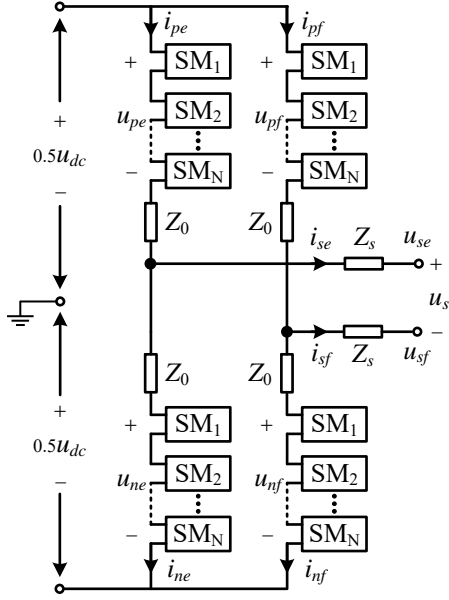


Fig. 14: MMC inverter topology

According to KVL, the voltage equation for the positive arm and negative arm can be written as

$$u_{sj} + Z_s i_{sj} + u_{pj} + Z_0 i_{pj} = 0.5u_{dc}, \quad (24a)$$

$$u_{sj} + Z_s i_{sj} - u_{nj} - Z_0 i_{nj} = -0.5u_{dc}, \quad (24b)$$

where  $u_{sj}(j = e, f)$  is the output voltage relative to the ground,  $Z_s i_{sj}$  is the voltage across the single-phase impedance,  $Z_0 i_{pj}$  and  $Z_0 i_{nj}$  are the impedance voltage in the positive arm and negative arm respectively.

The definition of differential voltage and common voltage is consistent with (14), and the following equation can be easily derived,

$$Z_{s0} i_{gj} = u_{diffj} - u_{sj}, \quad (25a)$$

$$Z_0 i_{cirj} = 0.5u_{dc} - u_{comj}. \quad (25b)$$

where  $Z_{s0} = Z_s + 0.5Z_0$ .

The primary purpose of inverter control is voltage tracking control. According to (25a), the output voltage of the two phases can be written as,

$$\begin{cases} u_{se} = u_{dife} - Z_{s0} i_{se} \\ u_{sf} = u_{diff} - Z_{s0} i_{sf} \end{cases} \quad (26)$$

The single-phase output voltage  $u_s = u_{se} - u_{sf}$ . The variable that can be controlled is the differential voltage of MMC inverter. Since the reference voltage is a sinusoidal signal with angular velocity  $\omega_0$ , the output voltage control adopts a proportional-resonant (PR) controller with a resonant frequency  $\omega_0$ .

$$\begin{aligned} (u_{dife} - u_{diff})^* &= \left( k_{p5} + \frac{k_{r5}s}{s^2 + \omega_0^2} \right) (u_s^* - u_s) \\ &+ u_s^* + Z_{s0} (i_{se} - i_{sf}) \end{aligned} \quad (27)$$

where  $u_s^*$  is the reference voltage from the upper droop controller, both the reference voltage  $u_s^*$  and impedance voltage drop

$Z_{s0} (i_{se} - i_{sf})$  are added as feed-forward compensations. In order to maximize voltage efficiency, the phase angle between  $u_{dife}^*$  and  $u_{diff}^*$  is set to  $180^\circ$ . The control diagram of AC output voltage is shown below.

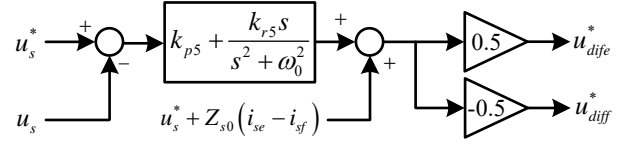


Fig. 15: Control diagram of AC voltage

Double-frequency circulating current also exists in single-phase MMC inverter. From (25b), the dynamic equation of the circulating current in MMC inverter can be written as:

$$\begin{cases} Z_0 i_{cire} = 0.5u_{dc} - u_{come} \\ Z_0 i_{cirf} = 0.5u_{dc} - u_{comf} \end{cases} \quad (28)$$

It can be seen that in single-phase MMC inverter, the common voltage can also be used to suppress circulating current. The difference is that the AC component in single-phase MMC inverter cannot be cancelled by summation, so a low pass filter is adopted to obtain the reference signal from the original circulating current,  $i_{cirj}^* = \text{LPF}(i_{cirj})$ . The reference common voltage can be calculated by

$$u_{comj}^* = 0.5u_{dc} - \left( k_{p6} + \frac{k_{i6}}{s} + \frac{k_{r6}s}{s^2 + 4\omega_0^2} \right) (i_{cirj}^* - i_{cirj}) \quad (29)$$

Based on the above equation, the control diagram of MMC inverter circulating current is presented in Fig. 16.

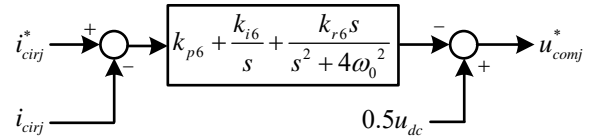


Fig. 16: Control diagram of circulating current in MMC inverter

The control of single-phase MMC inverter includes external output voltage control and internal circulating current control, which is similar to the control of three-phase MMC rectifier. The overall control scheme of MMC inverter is shown in Fig. 17.

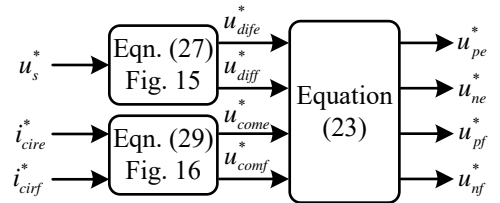
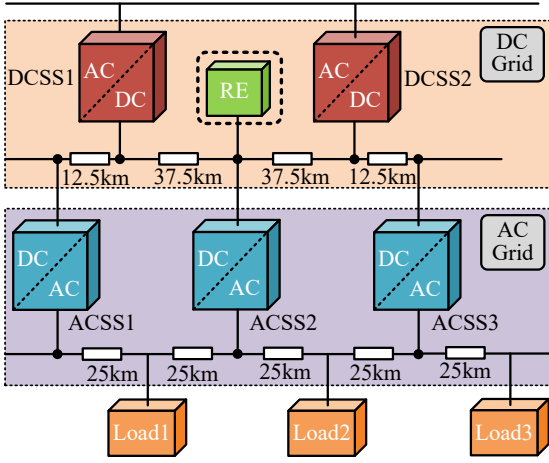


Fig. 17: Overall control diagram of the MMC inverter

## 5 Simulated System Operation

Due to the high flexibility of the proposed double-layer TPSS, the possible configurations are diverse and may become very complex. In this paper, a simplified double-layer DC/AC TPSS system is established in MATLAB/Simulink environment to verify its feasibility, as shown in Fig. 18. When the three-phase MMC rectifier



**Fig. 18:** Simulation model of a general double-layer DC/AC TPSS with renewable integration

and single-phase MMC inverter adopt the same configuration for each phase, the former has around 1.5 times the power of the latter. Assuming the average power supply distance for a MMC inverter is 50km, the average distance between adjacent rectifiers should be around 75km. In the simulation model, there are two parallel rectifiers together with a renewable source feeding three inverters. All the parallel converters are controlled by droop and inner voltage control strategy. Therefore, this system model is representative for a general double-layer DC/AC TPSS. Different from the top-down system design approach, a bottom-top simulation verification is carried out here. The main simulation parameters are listed in Table 1.

**Table 1** Simulation Parameters of Hybrid DC/AC TPSS

Parameter	Value
Grid voltage	110kV
DC TPSS voltage	20kV
AC TPSS voltage	27.5kV
DC line impedance	0.1 $\Omega$ /km
AC line impedance	(0.14+j0.21) $\Omega$ /km
Rated power of each AC-DC substation	18MW
Rated power of each DC-AC substation	12MW
Traction load power	5MW
Regenerative braking power	5MW
Maximum power of renewable energy	5MW
MMC arm inductance	20mH
MMC arm resistance	0.5 $\Omega$
MMC SM number	10
MMC SM capacitance	2mF
MMC SM capacitor voltage	2000V
Simulation step size	5 $\mu$ s

### 5.1 Performance evaluation for a single MMC converter

MMC converters play an important role in the proposed TPSS, and its performance directly determines the stability and reliability of system operation. From the system operation point of view, the output characteristics of MMC converters, especially voltage tracking performance, are the most important issue. In order to verify the external characteristics of MMC converters, a rectifier and an inverter are built respectively. When a 10MW step load is added to both of them, the external characteristics for them are shown in Fig. 19 and Fig. 20.

It can be seen that the DC bus voltage is pulled down slightly when a step load current is presented. The voltage quickly reaches a new steady state with no steady-state error. In the whole transient response period, voltage fluctuations are less than 5%. For the MMC inverter, the steady state can also be quickly reached after small fluctuations. The traditional PI controller cannot eliminate the steady-state error, but here it is shown that due to the introduction

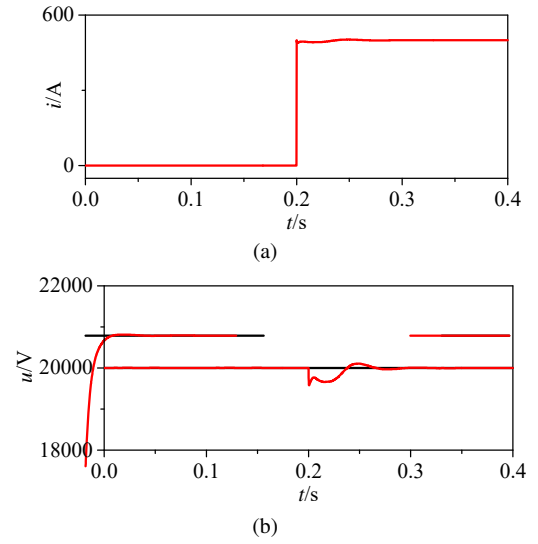


**Fig. 19:** External characteristics of the MMC rectifier. (a) Output current. (b) Output voltage.

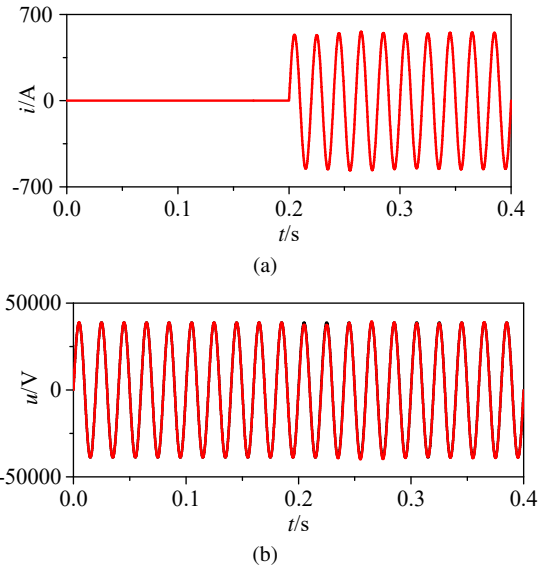


**Fig. 20:** External characteristics of the MMC inverter. (a) Output current. (b) Output voltage.

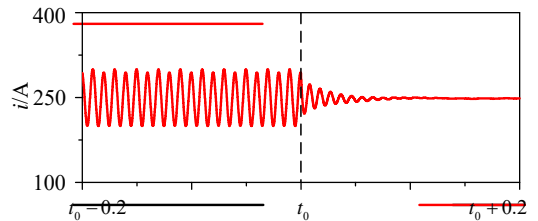


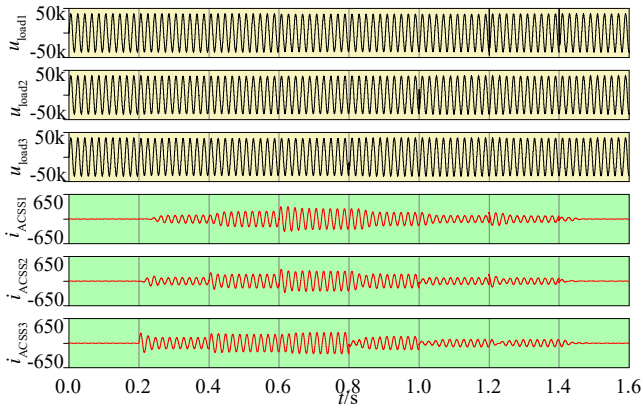
**Fig. 21:** Circulating current performance before and after the circulating current controller is applied.

of the resonant control loop, SSE-free tracking can be achieved. The step load is change actually a much worse case than the actual traction load changes in reality, but both the DC and AC voltages only fluctuate slightly and can return to the stable state with no error in a short time. Therefore, MMC control strategy in this paper shows reliable performance in voltage tracking.

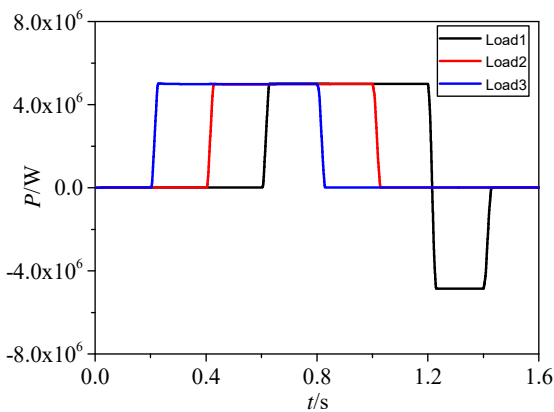
Further, since circulating current suppression is of great significance for loss reduction and efficiency improvement, taking phase  $e$  as an example, its circulating current suppression performance before and after adding the circulating current controller is also compared in Fig. 21. It is evident that, when the internal suppression algorithm is employed at  $t_0$ , the secondary harmonics in the circulating current will be eliminated, and only the effective dc component is retained.

## 5.2 AC-layer grid operation

Neutral sections are cancelled in the proposed TPSS, and all the MMC inverters are connected in parallel. Compared with normal AC microgrids, the biggest difference is the load profile. The change rate and range of traction loads are much higher than conventional microgrids, which puts a challenge on the stable operation of the proposed TPSS. To verify the performance of the proposed TPSS, a much worse scenario than actual traction loads is simulated. Within 0-0.2s, there is no load connected to the AC-layer grid. At 0.2s, 0.4s and 0.6s, load 3, 2 and 1 are connected in turn to emulate train starting process with increasing currents. At 0.8s, 1.0s and 1.2s, load 3, 2 and 1 are cut off in turn to emulate train braking process with decreasing currents. Note that the braking of load 1 is considered as a regenerative mode, which means a regenerative current will be injected into the TPSS during 1.2-1.4s.



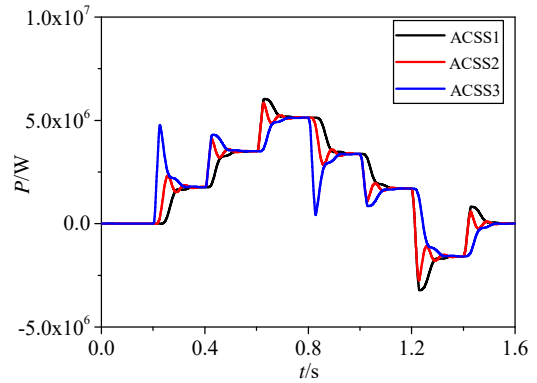
**Fig. 22:** Voltage and current waveform in AC-layer grid.



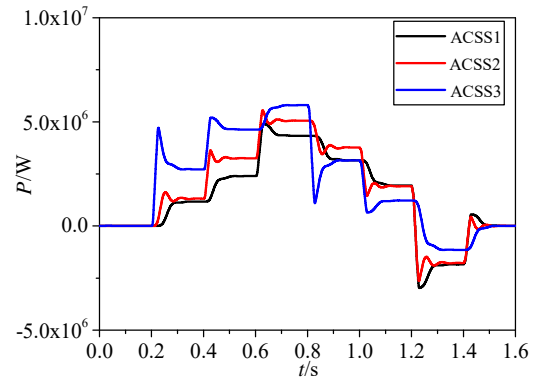
**Fig. 23:** Simulated traction load profiles.

Fig. 22 shows the voltage waveform at three load connection points and the output current of three inverters. It is shown that during the whole simulation process, load voltages at different locations remain largely unchanged. This is due to the good performance of voltage tracking control. Even when the traction loads change suddenly, its voltage fluctuates very slightly and stabilizes at around 27.5V (RMS) in a short time. As it is also shown in the current

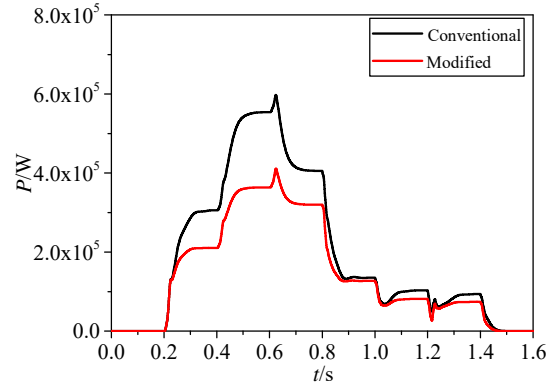
waveform, several converters share the power supply in the AC-layer traction grid. When the load changes suddenly, neighboring AC substations respond faster and provide more current in a short time. Gradually these burdens are shared with other converters and a system steady state is then achieved.



(a)



(b)



(c)

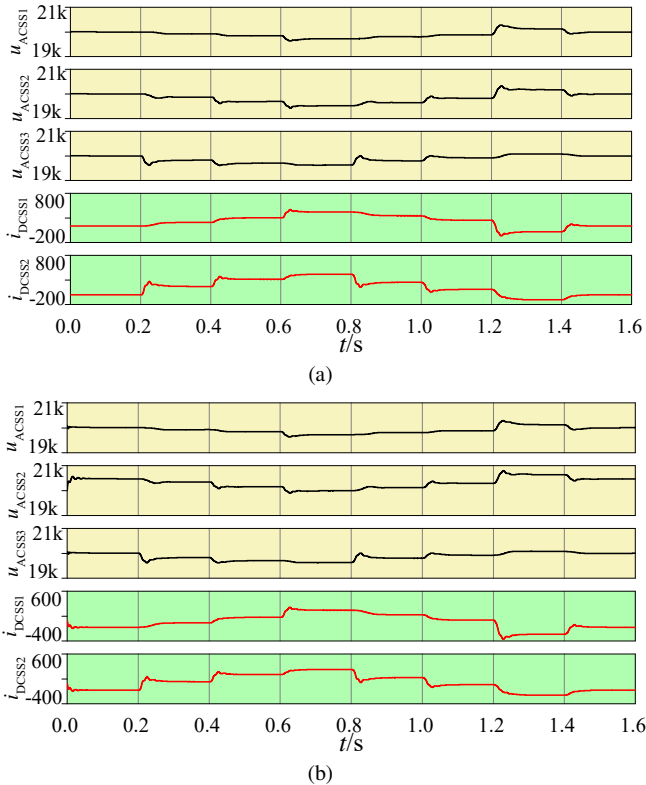
**Fig. 24:** Power outputs of ACSSs and transmission line losses. (a) Output power in conventional droop control. (b) Output power in modified droop control. (c) Line losses comparison.

Fig. 23 presents the measured traction load profiles. Each profile consists of three stages: acceleration, steady-state operation and deceleration. The only difference is that regenerative braking is considered in load profile 1. It is shown that all the three loads can operate at the given profiles throughout the process. Fig. 24 compares inverter power outputs under conventional droop control and modified droop control strategy. Note that, the sudden change of load power is mainly provided by its nearby substations in the beginning. While with the control effects of droop controller, energy redistribution can be achieved as shown from the dynamics of power sharing in Fig. 24. Both the conventional droop control and modified droop

control can enter a steady state stage after a short transient adjustment. Due to the decoupling of line resistance and inductance, the modified droop control strategy can achieve steady states in less time. While in terms of the line losses, it is shown that the overall line losses are reduced using modified droop control. When the traction load becomes the heaviest, line loss is reduced by more than 30%. It is worth noting that this is the result of automatic energy distribution, with all converters using the same droop parameters. This demonstrates the potential of the proposed droop control in further energy optimization operations.

### 5.3 DC-layer grid operation

In this proposed TPSS, each inverter is not powered by a single rectifier but connected to the DC-layer grid. In the DC grid, energy can flow freely, so all of the power demands from the AC layer will be met by parallel rectifiers in the DC layer. In the simulation model, the DC-layer network is supplied by two MMC rectifiers as well as a renewable energy source. Wind power, solar energy and some other renewable generations have the characteristics of intermittency and volatility, which bring challenges to maximum power point tracking (MPPT) control [41]. However, for their potential applications in future traction systems, the change rate of renewable energy is much slower than that of traction loads. Besides, batteries can also be integrated into renewable generation to further reduce output power fluctuations [42]. Thus, the transient MPPT process can be ignored, and renewable generation can be modeled as a controlled current source with a reference signal of  $P_{RE}/u_{dc}$ .



**Fig. 25:** Voltage and current waveform in DC-layer grid. (a)  $P_{RE} = 0$ . (b)  $P_{RE} = 5\text{MW}$ .

As the traction load changes, the energy demand is transferred from the AC-layer grid to the DC-layer grid. Thus, in DC bus, ACSS 1-3 are DC loads while DCSS 1-2 are DC power supply sources. Fig. 25 shows the DC load voltage waveform, namely  $u_{ACSS1}$ ,  $u_{ACSS2}$  and  $u_{ACSS3}$ , and the DC current waveform provided by DCSS 1 and 2. In general, the DC bus voltage with renewable power is slightly higher than that without renewable.

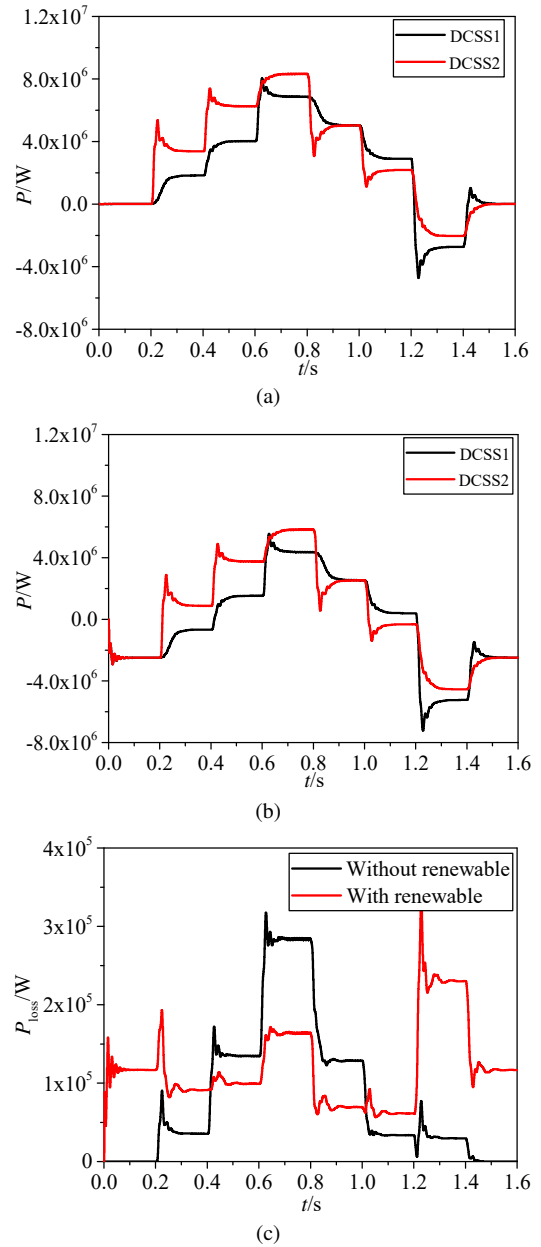


**Fig. 26:** Power outputs of DCSSs and transmission line losses. (a) Substation power when  $P_{RE} = 0$ . (b) Substation power when  $P_{RE} = 5\text{MW}$ . (c) Line losses comparison.

Since DC line resistance will inevitably cause voltage drop and secondary control is not the focus of this paper, it is acceptable to allow steady-state error within a certain range. For the case with renewable, the steady-state value of  $u_{ACSS2}$  is about 2.5% higher than  $u_{ACSS1}$  and  $u_{ACSS3}$  even when there is no load. This is because the generated energy from renewable generator is fed back to the utility grid via transmission line, so the bus voltage is slightly raised. For this case, the rectifier works as a grid-connected converter for renewable generation, as shown in its current waveform. Since renewable energy feedback is shared by multiple converters, system safety and reliability are greatly enhanced. When the dc load current changes, there is only a very small amount of load voltage overshoot and it can quickly reach the stable state. Power characteristics, including output power of DC substations and line losses, are compared in Fig. 26. It is shown that when the system is equipped with distributed renewable generators, the overall supply power of AC-DC converters decreases, and the maximum output power also decreases. This will benefit the DCSS life and reliability of power electronics. On the other hand, the reduction in DCSS power also means the renewable

energy is transmitted directly to traction loads, thus the efficiency of energy use is improved. As shown in Fig. 26(c), with the introduction of renewable energy, additional dc line losses will also be introduced in light load and regenerative braking cases, whose value is determined by the power of renewable and breaking generation and its location in the dc-layer grid. Note that, for busy railway cases, the introduction of renewable can reduce dc line losses, as the renewable energy can be directly transmitted to the traction loads.

#### 5.4 System Operation under Substation Fault

Compared to the traditional transformer based TPSS, the biggest challenge of power electronics based TPSS is system reliability. Therefore, the design of TPSS should consider fault-tolerant operation under substation fault, so as to improve system reliability. System operation under substation fault is of great significance for the future practical application of the proposed topology. A main characteristic of the double-layer DC/AC TPSS is that it can realize free energy flow and automatic energy distribution in different layers. This means that if either the rectifier or the inverter fails, its original energy conversion task can be reassigned to the surrounding converters, and a new energy flow path can be re-established automatically. Apart from the fact that the faulty substation cannot work, other converters in the proposed TPSS can continue to operate, which makes sense because it minimizes the impact of the failed substations and improves system reliability.

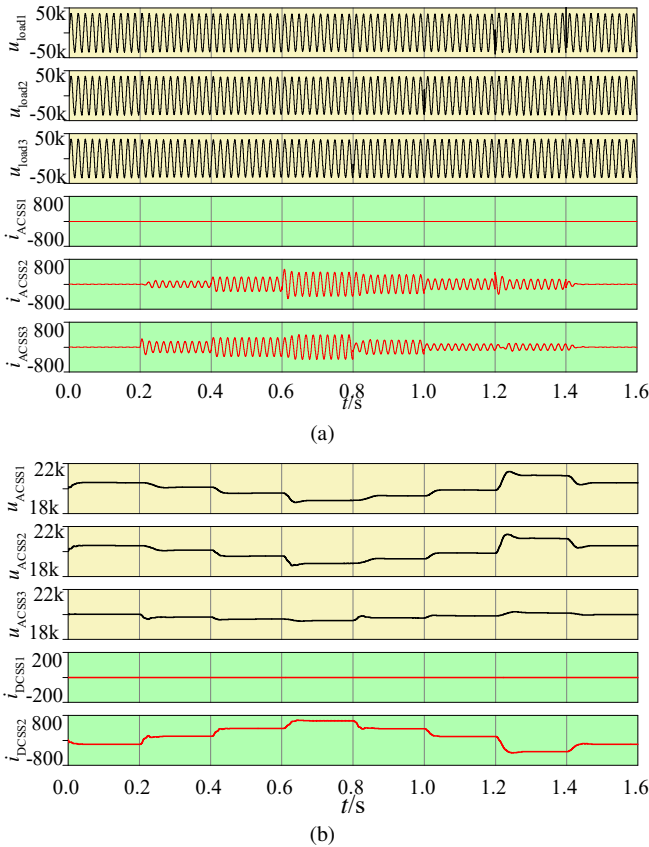


**Fig. 27:** Voltage and current waveform under substation fault. (a) AC load voltage and ACSS current profiles. (b) DC load voltage and DCSS current profiles

To verify the performance of the proposed TPSS under substation faults, a severe case where both ACSS1 and DCSS1 fail simultaneously is simulated, while traction loads are still consistent with the previous simulation. Fig. 27(a) and 27(b) show the load voltage and the substation current in the AC and DC layer respectively. It

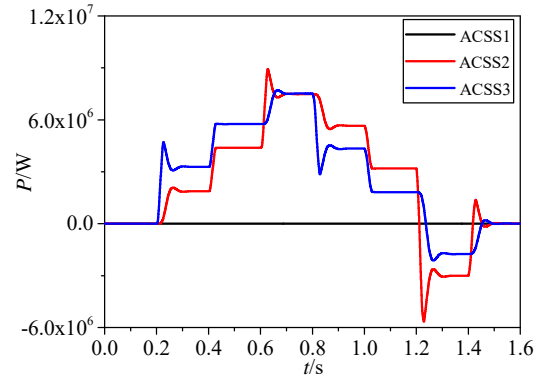


**Fig. 28:** Power outputs of ACSSs under substation fault.

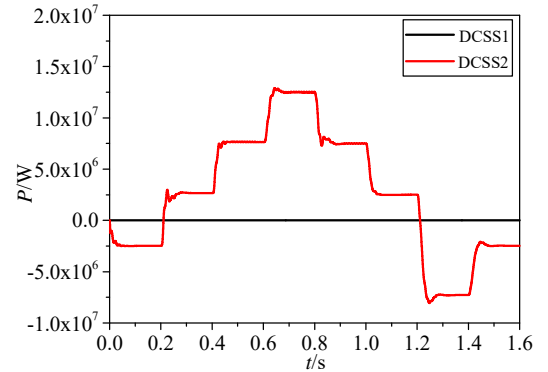


**Fig. 29:** Power outputs of DCSSs under substation fault.

is shown that although faults exist in both ACSS1 and DCSS1, the stable voltage support to the loads can still be guaranteed.

Fig. 28 compares the output power of three AC substations. It can be seen that the energy demand from the traction loads is shared by ACSS2 and ACSS3 automatically. During 0.6-0.8s, loads in AC-layer grid are symmetrical to the two ACSSs, so their steady-state output power is basically the same. Furthermore, the output power of rectifiers in DC-layer grid is shown in Fig. 29. Compared with Fig. 26(b), the power originally supplied by DCSS1 is automatically provided by DCSS2 and the renewable source, whose power is assumed to be half of the maximum. Therefore, even if multiple substations fail, the other substations can still operate normally and re-establish energy distribution, which greatly improves the system reliability.

## 6 Conclusion

Compared with the existing transformer based TPSS, the back-to-back converter based TPSS can eliminate neutral sections and improve power quality. This paper has further proposed a novel double-layer TPSS with renewable integration, which can achieve further development in system reliability, renewable integration and power matching. Meanwhile, the original advantages of the back-to-back topology are retained. Simulation results show that, (1) The designed MMC controller can perfectly track the voltage reference from the upper droop controller; (2) Compared with the traditional AC droop strategy, the proposed modified droop controller can achieve energy distribution faster and reduce line losses; (3) The designed DC droop controller can achieve the primary control of energy flow in DC-layer grid, and the integration of renewable generation in DC grid can directly provide energy for traction loads, which not only improves energy conversion efficiency but also reduces line losses; (4) Even when several substations fail at the same time, the whole system can still run smoothly, so the reliability of the proposed system can be guaranteed.

## 7 Acknowledgments

Yongfei LI would like to thank the China Scholarship Council for the financial support of two-year visiting study at University of Leeds.

## 8 References

- Gazafrudi, S.M.M., Langerudy, A.T., Fuchs, E.F., AlHaddad, K.: 'Power quality issues in railway electrification: A comprehensive perspective', *IEEE transactions on industrial electronics*, 2014, **62**, (5), pp. 3081–3090
- He, X., Shu, Z., Peng, X., Zhou, Q., Zhou, Y., Zhou, Q., et al.: 'Advanced cophase traction power supply system based on three-phase to single-phase converter', *IEEE Transactions on Power Electronics*, 2013, **29**, (10), pp. 5323–5333
- Zhang, D., Zhang, Z., Wang, W., Yang, Y.: 'Negative sequence current optimizing control based on railway static power conditioner in v/v traction power supply system', *IEEE Transactions on Power Electronics*, 2015, **31**, (1), pp. 200–212
- He, X., Peng, J., Han, P., Liu, Z., Gao, S., Wang, P.: 'A novel advanced traction power supply system based on modular multilevel converter', *IEEE Access*, 2019, **7**, pp. 165018–165028
- Krastev, I., Tricoli, P., Hillmans, S., Chen, M.: 'Future of electric railways: advanced electrification systems with static converters for ac railways', *IEEE Electrification Magazine*, 2016, **4**, (3), pp. 6–14
- Shu, Z., Xie, S., Li, Q.: 'Single-phase back-to-back converter for active power balancing, reactive power compensation, and harmonic filtering in traction power system', *IEEE Transactions on Power Electronics*, 2010, **26**, (2), pp. 334–343
- Shu, Z., Xie, S., Lu, K., Zhao, Y., Nan, X., Qiu, D., et al.: 'Digital detection, control, and distribution system for co-phase traction power supply application', *IEEE transactions on industrial electronics*, 2012, **60**, (5), pp. 1831–1839
- Dai, N.Y., Lao, K.W., Wong, M.C., Wong, C.K.: 'Hybrid power quality conditioner for co-phase power supply system in electrified railway', *IET Power Electronics*, 2012, **5**, (7), pp. 1084–1094
- Lao, K.W., Wong, M.C., Dai, N., Wong, C.K., Lam, C.S.: 'A systematic approach to hybrid railway power conditioner design with harmonic compensation for high-speed railway', *IEEE Transactions on industrial electronics*, 2014, **62**, (2), pp. 930–942
- Li, L., Wu, M., Wu, S., Li, J., Song, K.: 'A three-phase to single-phase ac-dc-ac topology based on multi-converter in ac electric railway application', *IEEE Access*, 2019, **7**, pp. 111539–111558
- Choi, B.Y., Kang, J.W., Kang, K.M., Lee, H., Lee, S.S., Won, C.Y.: 'A modified droop control method for parallel-connected three-phase inverter in railway auxiliary power supply'. In: 2019 IEEE Transportation Electrification Conference and Expo, Asia-Pacific (ITEC Asia-Pacific). (IEEE, 2019). pp. 1–6
- Adefarati, T., Bansal, R.: 'Integration of renewable distributed generators into the distribution system: a review', *IET Renewable Power Generation*, 2016, **10**, (7), pp. 873–884
- Alexander, A., Thathan, M.: 'Modelling and analysis of modular multilevel converter for solar photovoltaic applications to improve power quality', *IET renewable power Generation*, 2014, **9**, (1), pp. 78–88
- Mwasilu, F., Jung, J.W.: 'Potential for power generation from ocean wave renewable energy source: a comprehensive review on state-of-the-art technology and future prospects', *IET Renewable Power Generation*, 2018, **13**, (3), pp. 363–375
- Xiao, W., ElMoursi, M.S., Khan, O., Infield, D.: 'Review of grid-tied converter topologies used in photovoltaic systems', *IET Renewable Power Generation*, 2016, **10**, (10), pp. 1543–1551
- Akhter, M.N., Mekhilef, S., Mokhlis, H., Shah, N.M.: 'Review on forecasting of photovoltaic power generation based on machine learning and metaheuristic techniques', *IET Renewable Power Generation*, 2019, **13**, (7), pp. 1009–1023
- D'Arco, S., Piegari, L., Tricoli, P.: 'Comparative analysis of topologies to integrate photovoltaic sources in the feeder stations of ac railways', *IEEE transactions on transportation electrification*, 2018, **4**, (4), pp. 951–960
- Mingliang, W., Weiyang, W., Wenli, D., Huabo, C., Chaohua, D., Weirong, C.: 'Back-to-back pv generation system for electrified railway and its control strategy'. In: 2017 IEEE Transportation Electrification Conference and Expo, Asia-Pacific (ITEC Asia-Pacific). (IEEE, 2017). pp. 1–6
- Mitra, B., Chowdhury, B., Manjrekar, M.: 'Hvdc transmission for access to offshore renewable energy: a review of technology and fault detection techniques', *IET Renewable Power Generation*, 2018, **12**, (13), pp. 1563–1571
- Wang, M., Hu, Y., Zhao, W., Wang, Y., Chen, G.: 'Application of modular multilevel converter in medium voltage high power permanent magnet synchronous generator wind energy conversion systems', *IET Renewable Power Generation*, 2016, **10**, (6), pp. 824–833
- Ronanki, D., Williamson, S.S.: 'Modular multilevel converters for transportation electrification: Challenges and opportunities', *IEEE Transactions on Transportation Electrification*, 2018, **4**, (2), pp. 399–407
- Ma, F., Xu, Q., He, Z., Tu, C., Shuai, Z., Luo, A., et al.: 'A railway traction power conditioner using modular multilevel converter and its control strategy for high-speed railway system', *IEEE Transactions on Transportation Electrification*, 2016, **2**, (1), pp. 96–109
- Ma, F., Zhu, Z., Min, J., Yue, Y., He, X.: 'Model analysis and sliding mode current controller for multilevel railway power conditioner under the v/v traction system', *IEEE Transactions on Power Electronics*, 2018, **34**, (2), pp. 1243–1253
- Xu, Q., Ma, F., He, Z., Chen, Y., Guerrero, J.M., Luo, A., et al.: 'Analysis and comparison of modular railway power conditioner for high-speed railway traction system', *IEEE Transactions on Power Electronics*, 2016, **32**, (8), pp. 6031–6048
- Lei, M., Li, Y., Zhao, C., Li, Z., Xu, F., Gao, F., et al.: 'Full degree of freedom based control scheme of the single-phase direct ac-ac modular multilevel converter for railway power conditioning under asymmetric branch conditions', *IEEE Transactions on Industrial Electronics*, 2019, **67**, (3), pp. 1671–1683
- Bessegato, L., Ilves, K., Harnefors, L., Norrga, S., Östlund, S.: 'Control and admittance modeling of an ac/ac modular multilevel converter for railway supplies', *IEEE Transactions on Power Electronics*, 2019, **35**, (3), pp. 2411–2423
- Ramezani, M., Li, S., Sun, Y.: 'Combining droop and direct current vector control for control of parallel inverters in microgrid', *IET Renewable Power Generation*, 2016, **11**, (1), pp. 107–114
- Li, Y., Li, Y.W.: 'Power management of inverter interfaced autonomous microgrid based on virtual frequency-voltage frame', *IEEE Transactions on Smart Grid*, 2011, **2**, (1), pp. 30–40
- Hill, R., Brillante, S., Leonard, P.: 'Railway track transmission line parameters from finite element field modelling: Series impedance', *IEE Proceedings-Electric Power Applications*, 1999, **146**, (6), pp. 647–660
- Tan, P.C., Loh, P.C., Holmes, D.G.: 'Optimal impedance termination of 25-kV electrified railway systems for improved power quality', *IEEE Transactions on Power Delivery*, 2005, **20**, (2), pp. 1703–1710
- Li, Q.: 'New generation traction power supply system and its key technologies for electrified railways', *Journal of Modern Transportation*, 2015, **23**, (1), pp. 1–11
- Harnefors, L., Antonopoulos, A., Norrga, S., Angquist, L., Nee, H.P.: 'Dynamic analysis of modular multilevel converters', *IEEE Transactions on Industrial Electronics*, 2012, **60**, (7), pp. 2526–2537
- Bahrani, B., Debnath, S., Saedifard, M.: 'Circulating current suppression of the modular multilevel converter in a double-frequency rotating reference frame', *IEEE Transactions on Power Electronics*, 2015, **31**, (1), pp. 783–792
- Xu, Y., Xu, Z., Zhang, Z., Xiao, H.: 'A novel circulating current controller for mmc capacitor voltage fluctuation suppression', *IEEE Access*, 2019, **7**, pp. 120141–120151
- Bessegato, L., Harnefors, L., Ilves, K., Norrga, S.: 'A method for the calculation of the ac-side admittance of a modular multilevel converter', *IEEE Transactions on Power Electronics*, 2018, **34**, (5), pp. 4161–4172
- Cwikowski, O., Wood, A., Miller, A., Barnes, M., Shuttleworth, R.: 'Operating dc circuit breakers with mmc', *IEEE Transactions on Power Delivery*, 2017, **33**, (1), pp. 260–270
- Liu, Y., Huang, M., Zha, X., Ju, H.H.C.: 'Short-circuit current estimation of modular multilevel converter using discrete-time modeling', *IEEE Transactions on Power Electronics*, 2018, **34**, (1), pp. 40–45
- Bessegato, L., Ilves, K., Harnefors, L., Norrga, S.: 'Effects of control on the ac-side admittance of a modular multilevel converter', *IEEE Transactions on Power Electronics*, 2018, **34**, (8), pp. 7206–7220
- Wang, J., Han, X., Ma, H., Bai, Z.: 'Analysis and injection control of circulating current for modular multilevel converters', *IEEE Transactions on Industrial Electronics*, 2018, **66**, (3), pp. 2280–2290
- Samajdar, D., Bhattacharya, T., Dey, S.: 'A reduced switching frequency sorting algorithm for modular multilevel converter with circulating current suppression feature', *IEEE Transactions on Power Electronics*, 2019, **34**, (11), pp. 10480–10491
- Di.Vincenzo, M.C., Infield, D.: 'New maximum power point tracker for photovoltaic systems exposed to realistic operational conditions', *IET Renewable Power Generation*, 2014, **8**, (6), pp. 629–637
- de la Torre, S., González.González, J.M., Aguado, J.A., Martín, S.: 'Optimal battery sizing considering degradation for renewable energy integration', *IET Renewable Power Generation*, 2018, **13**, (4), pp. 572–577